20th AIAA Computational Fluid Dynamics Conference
27 - 30 June 2011, Honolulu, Hawaii

AIAA 2011-3062

Numerical Study of the Aerodynamic Characteristics of a Plunging Rigid Airfoil with Elastic Trailing-Edge Plate

Jing Qian* and Zhengke Zhang†
National Key Laboratory of Science and Technology on Aerodynamic Design and Research, Northwestern Polytechnical University, Xi'an, Shaanxi, 710072, P. R. China

Shijun Luo‡ and Feng Liu§
Department of Mechanical and Aerospace Engineering, University of California, Irvine, CA 92697-3975, USA

The fluid-structure coupling process of a plunging rigid airfoil with a thin elastic plate attached at the trailing-edge is simulated numerically by using unsteady potential flow source/vortex panel method and the Euler-Bernoulli beam vibration differential equation. The flow characteristics, the unsteady aerodynamic loads, especially the thrust effects of the plunging motion are computed. The beam vibration differential equation for the elastic deformation motion of the attached trailing-edge plate is solved by finite difference method and the simulation of fluid-structure interaction process is conducted by a loose coupling iterative method. The analysis of the computed unsteady aerodynamic forces (e.g., lift and thrust), the propulsion efficiency and the shed vortices in the wake reveals that a proper elasticity of the thin elastic plate attached will lead to an optimum thrust for the airfoil.

I. Introduction

As micro air vehicle (MAV, a vehicle whose scale is less than 20cm, can cruise more than 10 km and last more than 20 minutes) has some advantages such as the small size, etc., it may have vast application potentials in both military use like low-altitude military reconnaissance, battle field loss and casualty assessment, target searching, border patrol, communication relay, and biochemical weapons detection and civilian use such as traffic monitoring, , wildlife surveys, forest fire prevention, etc. The recent development, on the other hand, in microelectronics and micro-computer technology makes it possible to put the micro air vehicle into practical applications.

The flapping way that birds, insects and fishes fly or swim arouses researchers' great interests[1]. Although trying to mimic the motion of birds, insects and fish triggered the invention of the airplane, the airplane with fixed wings only adopted the birds' principle of gliding, while ignoring and abandoning the birds' propulsion style of flapping. When MAV's scale is below 15cm with conventional aerodynamic layout of fixed wing, it can not obtain enough lift-to-drag ratio and will be unable to fly normally due to the low Reynolds number. Therefore the flapping propulsion manner of birds and insects is picked up again and reconsidered. No matter how large the insects are in size, e.g., as large as in centimeter level or as small as in millimeter level, they have diverse sophisticated flight ability because of utilizing the flapping propulsion style. The flapping MAV which imitates the motion style of birds, insects and fishes has better flight performance, better maneuverability and agility and lower energy consumption than the MAV with fixed wings or rotors. The flying style of flapping wings is becoming the first choice for the configuration layout of MAV.

Consequently, the experimental and numerical studies on flapping-wing aircraft and the aerodynamic benefits of flapping wings are theoretically valuable and likely of great practical applications as well. Knoller[2] and Betz[3] noticed, respectively in 1909 and 1912, that flapping airfoil would produce thrust. In 1922, by experimental observations, Katzmayr[4] confirmed this phenomenon – the so-called Knoller-Betz effect. Since then, research on aerodynamic characteristics of flapping wings emerged and grew gradually. Early experimental and theoretical studies can be found in Refs. 5-7. Nowadays, with codes or commercial software (e.g., Fluent, CFX, etc.), the unsteady flow over rigid flapping wings can be easily solved by numerical simulation. Therefore, the flight performance of the rigid

* Graduate Student.
† Professor.
‡ Researcher.
§ Professor, Associate Fellow AIAA.

flapping wing has been understood well. However, there is great difference between the flexible flapping wing and the rigid flapping wing. During each beat cycle, birds can change their span by actively twisting and bending their wings to get greater thrust and reduce drag. They can passively adjust and adapt their wings to the change of the flow field to prevent flow from separation and increase lift-to-drag ratio, thus facilitating the unsteady motion such as landing or taking off[8]. The studies made by M.S. Triantafyllou，G.S. Triantafyllou and Yue[9] indicates that flexibility is crucial to fish's agility when swimming in water. Heathcote et al.[10] conducted an experiment of a plunging airfoil with flexible plate attached at the trailing edge in a still water tank and found that at zero free stream velocity, the elasticity of the plate has significant effect on the vortex street, thrust and lift. They used three different flexible plates with different elasticity. When Reynolds number is less than 10^4, the most flexible plate makes the airfoil produce the greatest thrust, the plate with moderate elasticity makes the airfoil produce moderate thrust, and the rigid plate produces the minimum thrust for the airfoil. When Reynolds number is greater than 10^4, the plate with moderate elasticity makes the greatest thrust. In addition, the "ratio of propulsive power to input power" produced by the plate with the largest elasticity is still the greatest in the three although it decreases sharply as Reynolds number increases while the "ratio of propulsive power to input power" for the rigid plate is always the smallest. Heathcote and Gursul[11] carried out further experiments with non-zero free stream velocity and obtained new results. Tang et al.[12] used SIMPLE family of algorithms to solve Navier-Stokes equations for incompressible flow field and used Euler-Bernoulli beam vibration differential equation to solve the elastic deformation vibration motion of the thin plate, and coupled simultaneously the solution of the fluid flow with the computation of the structure deformation motion. The computational results show that the deformation caused by aerodynamic loading of the plunging airfoil modifies the effective angle of attack, thus leading to significant changes in lift and drag. The variation of elastic deformation displacement with time is consistent with the experimental observation of Heathcote and Gursul[11].

The numerical simulation of the unsteady flow field over the flexible flapping wing involves the deformation motion of the structure as well as the coupling with the flow field solution, thus being a complicated problem. Elastic deformation of flexible thin plate obviously increases the workload and levels of difficulty in computations. Even for flow field over a rigid flapping wing by solving Euler or Navier-Stokes equations complex grids and the readjustment of grids at each time step are needed. If the elastic deformation is taken into account, the re-generation of grids fitting the elastic deformation requires further treatment, besides, the deformation motion have to be solved too at each time step and must be coupled with the flow field solution, thus the computational workload is multiplied. In contrast, the panel method in potential flow does not require grid generation, therefore greatly improving the computational efficiency. In low speed case, the computational results obtained by potential flow panel method do not deviate much from experimental results. Anderson[13], Anderson et al.[14] compared the water tunnel experimental results of NACA0012 airfoil with a nonlinear incompressible potential flow computational results, and found that the experimental results agree well with the computed results if there is no apparent leading-edge vortices emerging. When an airfoil vibrates at high frequencies and low amplitudes, the effects of leading-edge separation vortices on aerodynamic characteristics will be small[15].

On the other hand, it is difficult to accurately describe the elastic deformation of a thin plate, that is, the deformation of the plate depends on the inertial force, the aerodynamic force and the elastic force. The inertial force is given, while the aerodynamic force and the elastic force are associated with the deformation and motion of the thin plate, thus undoubtedly making the calculation of the deformation even more difficult and complex. There are two basic ways for solving this aeroelasticity problem, namely the tight coupling method and the loose coupling method. In the tight coupling method, the deformation is calculated using the unconverged aerodynamic force, and then is input into the iteration process of the flow field solution and the calculation of the aerodynamic force. The process goes on until both the deformation and the aerodynamic force converge. In the loose coupling method, deformation is calculated only after the aerodynamic force converges, then the deformation is used for recalculating the aerodynamic force, the coupling proceeds until the deformation converges.

Therefore the present paper selects the potential flow source/vortex panel method to calculate flow field properties and aerodynamic characteristics of a flapping airfoil at high frequencies and low amplitudes, thus guaranteeing enough accuracy and much higher computational efficiency than the method of Euler equations or Navier-Stokes equations. At the same time, a thin flexible plate is attached to the rigid airfoil trailing edge and the airfoil-plate blended body is chosen as the model in the computation. Besides, the thin plate is regarded as an elastic beam and its elastic deformation motion is simulated numerically by solving Euler-Bernoulli beam vibration differential equation. The effect of the elastic deformation motion of the flexible plate on the flow field and aerodynamic force, especially on thrust is investigated intensively. The flow field is calculated by the unsteady potential flow panel method. The convergence of the interaction process of fluid flow / structure elastic deformation is guaranteed by using a loose coupling method[16].

II. Method for Flow Field Computation

The unsteady potential flow panel method described in Ref. 17 is used to calculate the unsteady aerodynamic loads on airfoils. In Ref. 17, it is assumed that the shed vorticity does not become free vortex directly in each time step, but is firstly distributed on a virtual small straight line wake element (shed vorticity panel) attached as an extra additional panel to the trailing edge. At next time step, all the vorticity on this virtual additional panel becomes a free vortex and is shed into the wake of the airfoil (see Fig. 1). In the present paper, an extra elastic thin plate is added to the trailing edge of the original airfoil to form an airfoil-plate combination as shown in Fig.1.

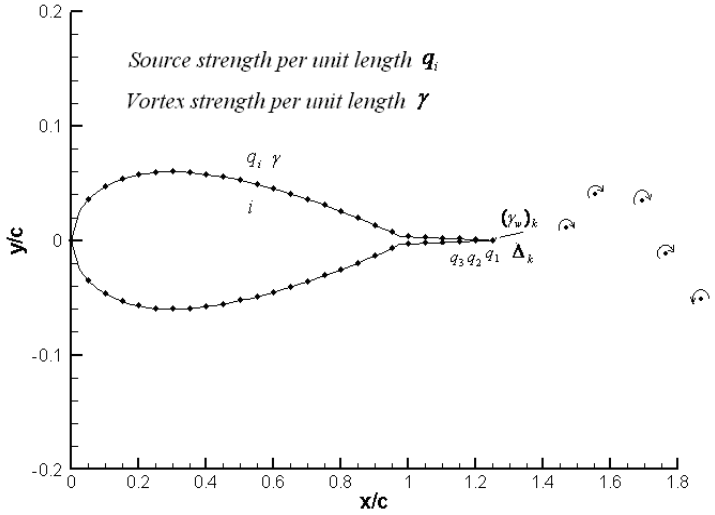

Figure 1 Schematic diagram of the potential flow panel method

According to Helmholtz's vortex theorems, at *k*th time step, the total circulation around the airfoil plus the vortex strength on the shed vorticity panel should be equal to the total circulation around the airfoil in the previous time step

$$\Delta_k \left(\gamma_w\right)_k + \Gamma_k = \Gamma_{k-1} \tag{1}$$

where the subscript *k* refers to the time step, Γ_k is the total circulation around the airfoil at time step *k*, $\left(\gamma_w\right)_k$ the vortex strength per unit length on the shed vorticity panel, and Δ_k the length of the shed vorticity panel at time step *k*.

Boundary conditions include the flow tangency conditions at the *n* panel control points, the Kutta condition of pressure equilibrium at the trailing edge panels and an orientation and length condition of the shed vorticity panel. The flow tangency conditions mean that at each of the *n* panels, the normal velocity of the fluid at the midpoint of panels equals the normal velocity of the object surface.

The orientation and length condition of the shed vorticity panel means that the angle Θ_k between the shed vorticity panel and the free stream direction and the length Δ_k of the shed vorticity panel must obey the following conditions

$$\tan\Theta_k = \frac{(V_w)_k}{(U_w)_k} \tag{2}$$

$$\Delta_k = (t_k - t_{k-1})\sqrt{(U_w)_k{}^2 + (V_w)_k{}^2} \tag{3}$$

where $(U_w)_k, (V_w)_k$ are the total velocity components at the midpoint of the shed vortictiy panel in the *x* and *y* directions, respectively.

The essence of the Kutta condition means the continuity of pressure on upper surface and lower surface at the trailing edge, that is $p_1/\rho = p_n/\rho$, where the subscript 1 represents the lower surface panel immediately ahead

of the trailing edge, and the subscript *n* represents the upper surface panel immediately ahead of the trailing edge. From unsteady Bernoulli's equation

$$\frac{\partial \varphi_1}{\partial t} + \frac{V_1^{\ 2}}{2} + \frac{p_1}{\rho} = \frac{\partial \varphi_n}{\partial t} + \frac{V_n^{\ 2}}{2} + \frac{p_n}{\rho} \tag{4}$$

The pressure at the trailing edge should be single-valued, an approximation of the single-valued condition can be expressed as $p_1 / \rho = p_n / \rho$, then from Eq. (4), the following equation can be obtained

$$(V)_1^{\ 2} - (V)_n^{\ 2} = 2[\frac{\partial \varphi_n}{\partial t} - \frac{\partial \varphi_1}{\partial t}] = 2[\frac{\partial \Gamma}{\partial t}] = 2[\frac{l_k \gamma_k - l_{k-1}\gamma_{k-1}}{t_k - t_{k-1}}] \tag{5}$$

where φ_1、φ_n are the velocity potential on the 1st panel and the *n*th panel, respectively, l_k is the perimeter of the airfoil at time step *k*, γ_k is the vortex strength per unit length at time step *k*, t_k is the time at time step *k*, Γ is the total circulation around the airfoil.

With the source strength and vortex strength distributions obtained, the tangential fluid velocity of each panel can be calculated by superimposing the contributions of the free stream, the source distributions, the vortex distributions and the additional shed vorticity panel. Then the pressure distribution can be calculated by using the unsteady Bernoulli's equation and finally, the lift and drag are obtained by integrating the pressure along the airfoil surface.

III. Structure Solver

The thin elastic plate attached to the trailing edge of a rigid airfoil is simplified to a cantilever whose motion relative to the rigid airfoil caused by elastic deformation should obey the following differential equation of the Euler-Bernoulli beam vibration

$$\left(IE \frac{\partial^4 w}{\partial x^4} \right) + \rho_s b \frac{\partial^2 w}{\partial t^2} = f(x,t) \tag{6}$$

where w is the displacement in the direction perpendicular to the chord (*x* direction), ρ_s the plate density (i.e., mass per unit volume), b the plate thickness, *E* the Young's modulus of material, *I* the moment of inertia of the plate cross sections, $f(x,t)$ the distributed load per unit length including inertial force acting on the plate due to the oscillating motion of the rigid airfoil and the pressure force which fluid exerts on the plate.

Equation (6) can be nondimensionalized to the following equation

$$\left(\overline{IE} \frac{\partial^4 \overline{w}}{\partial \overline{x}^4} \right) + \overline{\rho}_s \overline{b} \frac{\partial^2 \overline{w}}{\partial \overline{t}^2} = \overline{f}(\overline{x}, \overline{t}) \tag{7}$$

where

$$\overline{\rho}_s = \frac{\rho_s}{\rho_f}, \quad \overline{b} = \frac{b}{c}, \quad \overline{E} = \frac{E}{\rho_f U_\infty^2}, \quad \overline{I} = \frac{I}{c^3} = \frac{1}{12}(\overline{b})^3, \quad \overline{f}(x,t) = \frac{f(x,t)}{\rho_f U_\infty^2}$$

c is the chord length of the airfoil, ρ_f is the fluid density, U_∞ is the free stream velocity.

Discretizing Eq. (7) with a second-order implicit difference scheme[18] leads to the following difference equation

$$\begin{aligned} &\overline{\rho} \frac{b_j}{c} \frac{2\overline{w}_j^{n+2} - 5\overline{w}_j^{n+1} + 4\overline{w}_j^{n} - \overline{w}_j^{n-1}}{\Delta \overline{t}^{\,2}} + \\ &\frac{1}{12}(\frac{b_j}{c})^3 \overline{E} \frac{(\overline{w}_{j+2}^{n+2} - 4\overline{w}_{j+1}^{n+2} + 6\overline{w}_j^{n+2} - 4\overline{w}_{j-1}^{n+2} + \overline{w}_{j-2}^{n+2})}{\Delta \overline{x}^4} = \overline{f}_j^{n+2} \end{aligned} \tag{8}$$

The boundary conditions for solving the motion the vibrating plate can be expressed as: (1) at the fixed end of the plate, the displacement and its first derivative are both zero; (2) at the free end, both the second and third derivatives of the displacement are zero since there is no concentrated load or moment acting there.

Discretizing the boundary conditions and combing with the discretized Eq. (8) leads to a system of equations which is solved simultaneously to obtain the plate displacement (i.e., deformation). In order to verify the scheme and

the code, a uniform load varying sinusoidally with time is selected. The result of the numerical computation agrees well with that of the theoretical solution[19], showing that the difference equation (8) is of sufficient accuracy.

IV. Fluid-Structure Coupling Procedure

The loose coupling method[16] is used to carry out the fluid-structure coupling process. In the process the deformation is computed only after the flow field converges. Then the deformation is taken into account to modify the airfoil geometry to a new shape and re-solve the flow field to obtain the aerodynamic forces. The process is repeated till the deformation converges.

The coupling procedure in each time step for the fluid-structure interaction is iterated in the following way as sketched in Fig. 2:

(1) Receive the new airfoil shape from the structure solver (in the first time step, use the initial airfoil shape).
(2) Solve the flow field on the updated airfoil shape and iterate till the orientation and the length of the shed vorticity panel converge (sub-iteration is needed in the flow solver).
(3) Transfer the load from the flow solver to the structure solver.
(4) Solve the structural deformation by sub-iteration till the deformation convergent limit is reached.
(5) If the difference between present and previous deformation is less than the convergent limit, stop iteration.

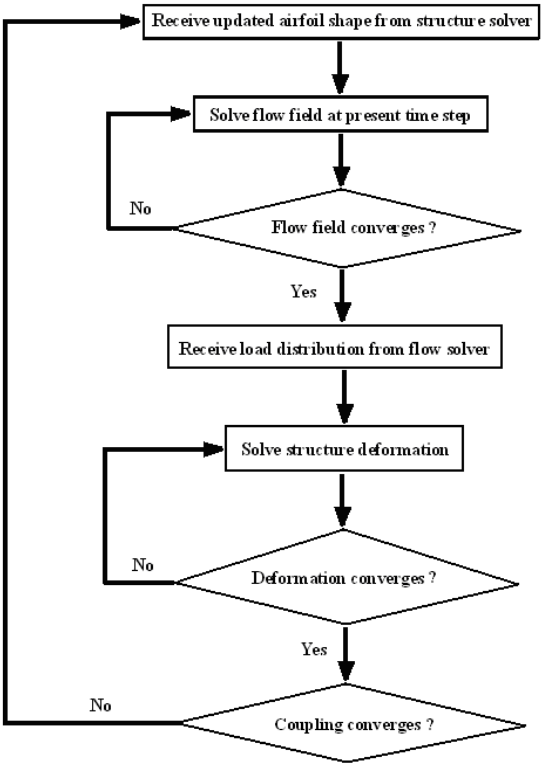

Figure 2 Flow chart of the fluid-structure coupling procedure

V. Results and Analysis

The NACA 0012 airfoil with an elastic thin plate of 25% chord length attached to the trailing edge is selected as the computational model. The joint between the original airfoil and the plate is smoothed with a fourth-order Bezier curve as shown in Fig. 3. In all the computational cases, the rigid part of the body (the original airfoil) is in a plunging motion in vertical direction and the incoming flow is in the horizontal direction and the upward-stroke and down-ward stroke of the plunging motion in each cycle are the sinusoidal function expressed as follows

$$\bar{h}(t) = \bar{h}_a \sin(kt) \tag{9}$$

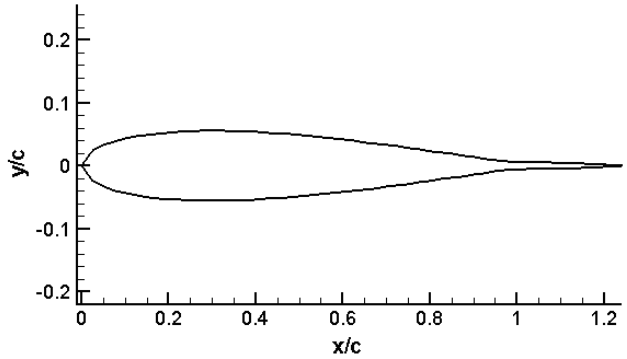

Figure 3 NACA0012 airfoil with a thin plate of 25% chord length

where $\overline{h} = h/c$ is the nondimensional displacement, h is displacement of the plunging airfoil in *y* direction, $\overline{h}_a$ is the nondimensional amplitude, $k = \omega c / U_\infty$, ω is the angular frequency of the sinusoidal plunging motion. In all the computational cases in this paper, $\overline{h}_a$=0.018, *k*=4.3, the dimensionless plate thickness $\overline{b} = b/c$ =0.001 and the dimensionless plate density $\overline{\rho}_s = \rho_s / \rho_f$ =1500 are chosen.

A. Vibration of Elastic Thin Plate

In order to examine how the elastic plate vibrates, we focus mainly on the motion of the rear end of the thin plate (i.e., the trailing edge of the airfoil-plate blended body, and we still will use "trailing edge" to represent the rear end of the plate). Figure 4 presents the displacement variation of the plate trailing edge with time relative to the airfoil leading edge (the left-hand side ordinate (longitudinal coordinate) in the figure) under different dimensionless Young's modulus values $\overline{E}$ = 6×10^7, 8×10^7, 1×10^8, 1.4×10^8, 2.0×10^8. It can be seen from the figure that the amplitude of the vibration first increases with the modulus until hitting a maximum at $\overline{E}$ =1×10^8, and then decreases with the modulus. Besides, different values of the modulus lead to different phases of the plate vibration, with $\overline{E}$ increasing, the time point at which the displacement reaches its peak marches backward gradually (that is, moves in the direction of decreasing time). This vibration mode is in good agreement with the result observed by Heathcote et al.[10,11], and is close to the computed result of a relative plate thickness of 0.00056 presented in Tang et al.'s paper[12]. The solid line labeled "Rigid" in Figure 4 represents the motion of a rigid plate relative to the airfoil leading edge. Besides, the oscillating motion of the rigid fore part of the airfoil itself (i.e., the rigid part of the airfoil-plate blended body) relative to the earth-attached coordinate system is also given in Figure 4 as labeled by the symbol "LE" for comparison using the right-hand side ordinate (vertical coordinate).

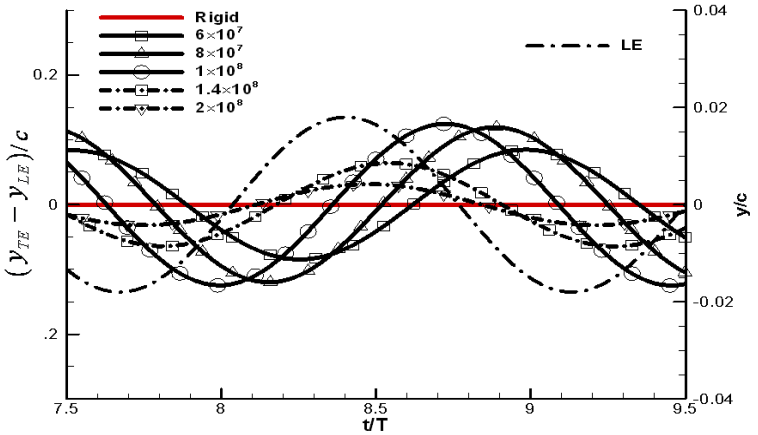

Figure 4 Variation of elastic plate trailing edge displacement with time

B. Influence of Elastic Thin Plate on Aerodynamic Forces

Figure 5(a), (b) shows the calculated variation of the drag and lift coefficients of the airfoil-plate blended body with time under four different plate modulus values (including the rigid one) as well as that of the single NACA 0012 airfoil. It is seen that that the lift coefficient and drag coefficient vary in an approximate sinusoidal manner with time. The manner of the variation is very close to the results computed by Tang et al.[12]. The drag of the single airfoil oscillates the least in amplitude.

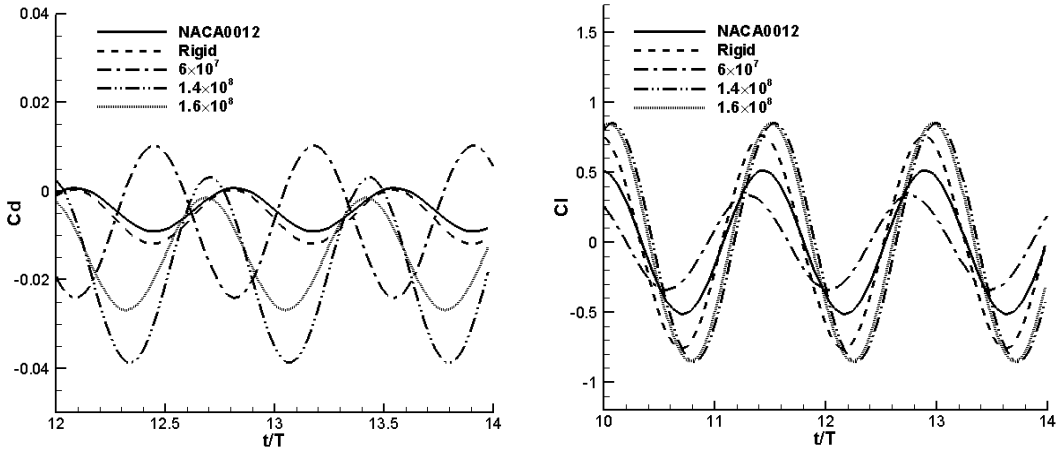

(a) Drag coefficient variation with time (b) Lift coefficient variation with time

Figure 5 Variation of drag and lift with time under different Young's modulus values

If the drag coefficient and lift coefficient under each dimensionless Young's modulus of the trailing plate (including the rigid plate) are averaged over a period of time, then the time-averaged drag coefficients and lift coefficients under different Young's modulus are obtained. The results are shown in Fig. 6(a), (b) compared with the results of the single rigid NACA 0012 airfoil. It can be found from Fig. 6(a) that in all computational cases, the airfoil time-averaged drag coefficient is negative, that is, the flapping wing with flexible trailing-edge plate seems to be able to produce thrust. Besides, the time-averaged drag coefficient decreases with $\overline{E}$ first when $\overline{E}$ is less than 10^8 and then increases with $\overline{E}$ when $\overline{E}$ is greater than 10^8. Thus at $\overline{E}=10^8$, the time-averaged drag coefficient comes to a minimum value (a maximum absolute value), meaning a maximum average thrust coefficient. The way in which the drag coefficient varies with the Young's modulus is in agreement with the experimental results obtained by Heathcote et al.[10]. The time-averaged drag coefficient of the airfoil with a rigid plate and that of the single NACA 0012 airfoil are the two largest in all cases as shown by the dashed line and the dash-dot line, respectively, in Fig. 6(a). It is obvious that the elastic thin plate can improve the propulsive thrust and there exists an optimum Young's modulus value at which the thrust reaches its maximum. From Fig. 6(b) it is seen that the time-averaged lift coefficient is zero for all computational cases. (The time-averaged lift coefficient of the rigid fore part-rigid plate blended body or the rigid single NACA 012 airfoil is obviously zero and thus not presented in Fig. 6(b).)

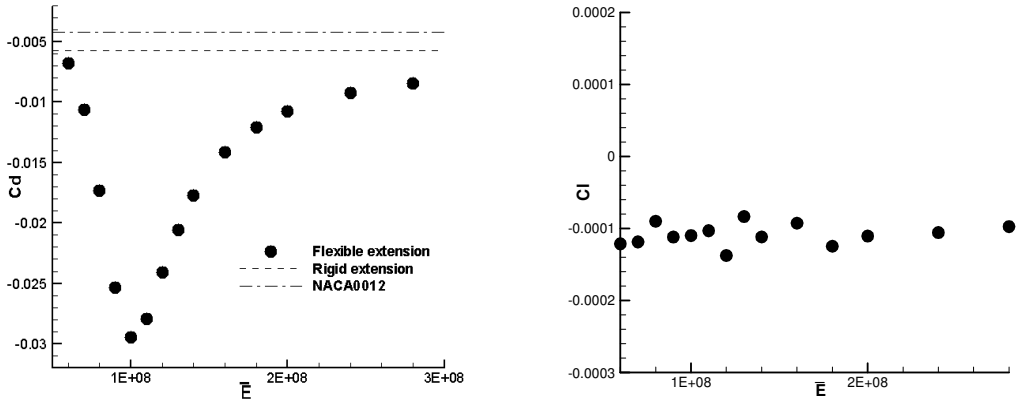

(a) Time-averaged drag coefficient (b) Time-averaged lift coefficient

Figure 6 Time-averaged drag and lift coefficient under different Young's modulus values

C. Drag Coefficient Correction

Viscosity is neglected in potential flow theory thus the drag obtained by the panel method is only the pressure drag instead of the total drag. The total drag should be the pressure drag plus the viscous drag, while net thrust (usable thrust) should be negative total drag instead of only the negative pressure drag. For simplicity without too much loss of accuracy, the airfoil is regarded as a flat plate to calculate the friction drag using boundary layer theory results[20].

When the boundary layer is laminar, the surface friction drag coefficient per unit length based on the well-known Blasius solution[20] is

$$C_f = 2 \times 1.328 \mathrm{Re}_c^{-1/2} \tag{10}$$

When the boundary is turbulent, the surface friction drag coefficient per unit length[20] is

$$C_f = 2 \times 0.074 \mathrm{Re}_c^{-1/5} \tag{11}$$

The Reynolds number Re for the airfoil-plate blended body is assumed to be 6.25×10^5. At this Re, the friction drag coefficient for laminar boundary layer and turbulent boundary layer, respectively, can be calculated and further the drag coefficient can be corrected.

Figure 7(a), (b) demonstrates the total (i.e., friction-corrected) time-averaged drag coefficient modified respectively by laminar friction drag and turbulent friction drag and its variation with nondimensional Young's modulus. The friction-corrected drag coefficients for the airfoil-rigid-plate blended body and the single rigid NACA 0012 airfoil are also presented as well. It can be seen from the figure that when the plate is rigid (dashed line) or for the single rigid NACA 0012 airfoil (dash-dot line), the time-averaged drag coefficient is positive, that is, the single rigid airfoil or rigid airfoil fore part - rigid trailing-edge plate blended body is difficult to produce net thrust (usable thrust). For elastic trailing-edge plate, there exists an interval of nondimensional Young's modulus values in which the time-averaged drag coefficient is negative, and a suitable value of $\overline{E}$ (i.e., $\overline{E}=10^8$) can be found to produce maximum negative time-averaged drag coefficient, i.e., the maximum thrust. This result is in agreement with the experimental results of Heathcote et al.[10].

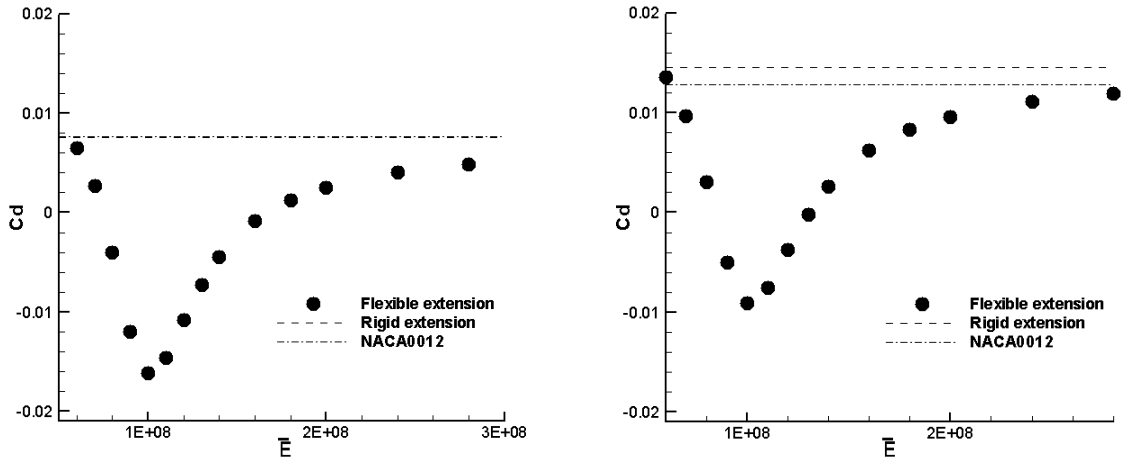

（a）Laminar friction corrected drag (b) Turbulent friction corrected drag

Figure 7 Time-averaged drag coefficient dependency on non-dimensional Young's modulus (Re=6.25×10^5)

D. Propulsive Efficiency

The propulsive efficiency can be defined as the ratio of propulsive power produced by the airfoil to the total mechanical power input to the airfoil, i.e.[21, 22],

$$\eta = \frac{\mathrm{P}_{propul}}{\mathrm{P}_{input}} = \frac{\mathrm{T}U_\infty}{\mathrm{P}_{input}} = \frac{\mathrm{T}U_\infty / \left(\frac{1}{2}\rho_\infty U_\infty^2 c U_\infty\right)}{\mathrm{P}_{input} / \left(\frac{1}{2}\rho_\infty U_\infty^2 c U_\infty\right)} = \frac{C_t \cdot 1}{C_\zeta} = \frac{C_t}{C_\zeta} \tag{12}$$

where T is the thrust, TU_∞ can be regarded as the propulsive power, $C_t = T / \frac{1}{2}\rho_\infty U_\infty^2 c$ is the time-averaged thrust coefficient, i.e., negative time-averaged total drag coefficient, C_ζ is the input power coefficient and can be computed by

$$C_\zeta = \frac{P_{input}}{\frac{1}{2}\rho_\infty U_\infty^2 c U_\infty} = -\frac{c}{U_\infty}\frac{1}{\tau}\int_0^1 \left[\oint C_p \frac{d\bar{h}(x,t)}{d\bar{t}} d\bar{x} \right] d\bar{t} \tag{13}$$

Figure 8(a), (b) gives the propulsive efficiency of the airfoil-plate blended body obtained from the friction-corrected thrust and its dependency on the nondimensional Young's modulus of the trailing-edge plate. Obviously, there exists an optimum Young's modulus value (i.e., $\overline{E} = 10^8$ in the figure) which produces the maximum propulsive efficiency.

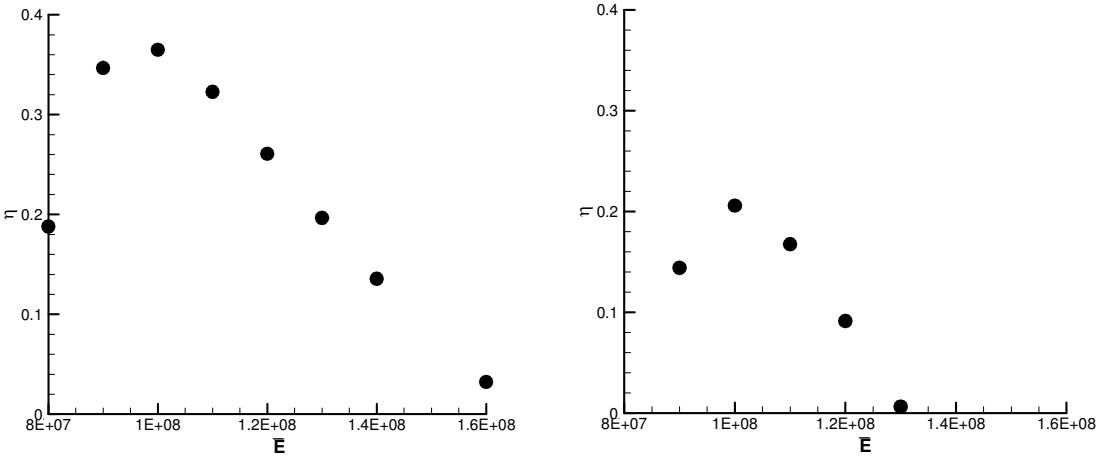

(a) Efficiency with laminar friction corrected (b) Efficiency with turbulent friction corrected

Figure 8 Airfoil propulsive efficiency dependency on nondimensional Young's modulus

E. Wake Vortices

Different values of Young's modulus of the attached thin plate will produce different shed vortex distributions in wake. Figure 9(a), (b), (c), (d), (e), (f), (g) exhibits the shed vortex distribution at $\overline{E}$ =8×10^7, 9×10^7, 1×10^8, 1.4×10^8, 2.4×10^8, 2.8×10^8, respectively, as well as that produced by the rigid plate where each point is a point vortex. The computed wake vortex distribution of the single rigid NACA 0012 airfoil is also presented as shown in Figure 9(h). The color of each point vortex represents the magnitude and sign of the vortex strength (i.e., circulation) there. From the figure, it can be seen that the point vortex with a circulation positive (clockwise rotation) in direction and large in magnitude periodically gathers immediately below the center line (y=0), while the one with a circulation negative in direction (counterclockwise rotation) and large in magnitude periodically gathers immediately above the center line (y=0). The vortices with smaller magnitude of circulation are farther away from the centerline. Therefore, the velocity of the flow field near the centerline is significantly greater than the free stream velocity. The features and manner of the circulation distribution in the wake are exactly in agreement with those obtained in the theoretical analysis and experimental observations by Jones, Dohring and Platzer[6], and are similar to the experimental results of Heathcote et al. [10,11]. Comparing Fig. 7(a) and Fig. 9(c) reveals that when $\overline{E} = 10^8$, the average thrust reaches the maximum and the maximum absolute value of circulation is the greatest among all the six modulus values as well as the rigid plate case and the single rigid NACA 0012 airfoil case. Thus, the greater the maximum absolute value of the circulation of the wake point vortex distribution is, the greater the average thrust coefficient is.

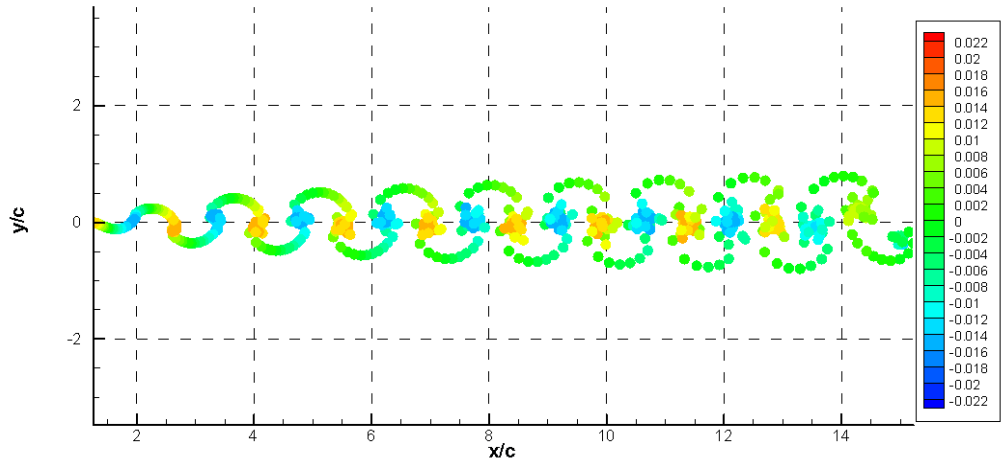

(a) $\overline{E} = 8 \times 10^7$

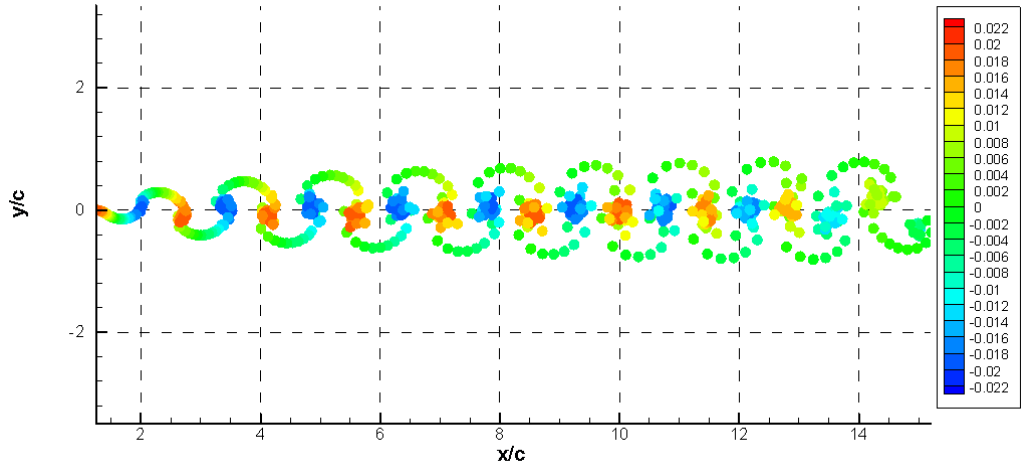

(b) $\overline{E} = 9 \times 10^7$

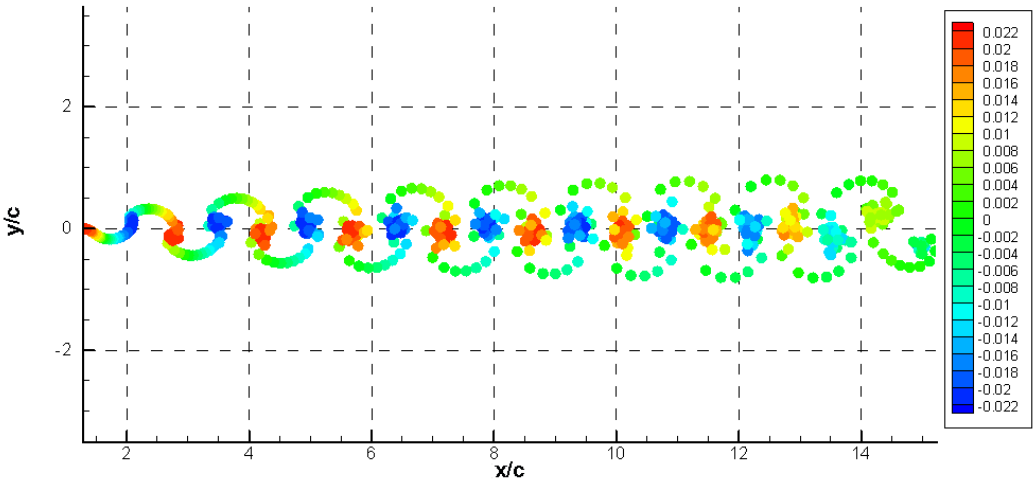

(c) $\overline{E} = 10^8$

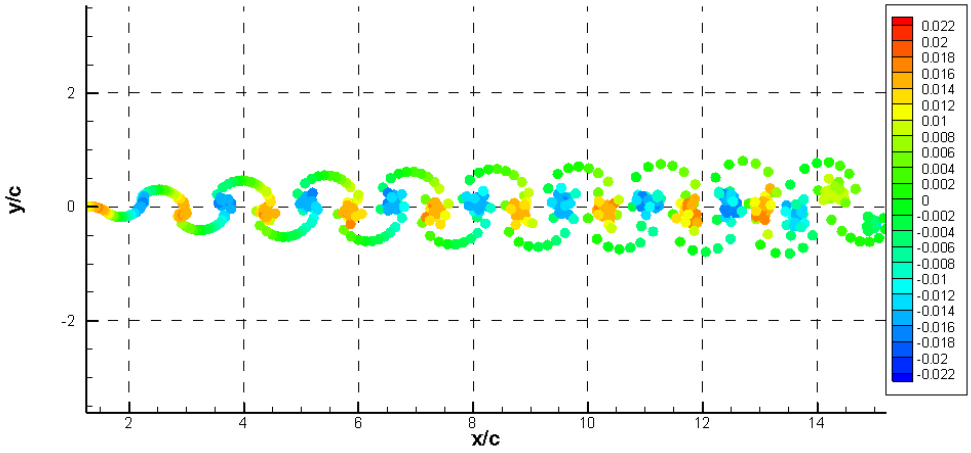

(d) $\overline{E} = 1.4 \times 10^8$

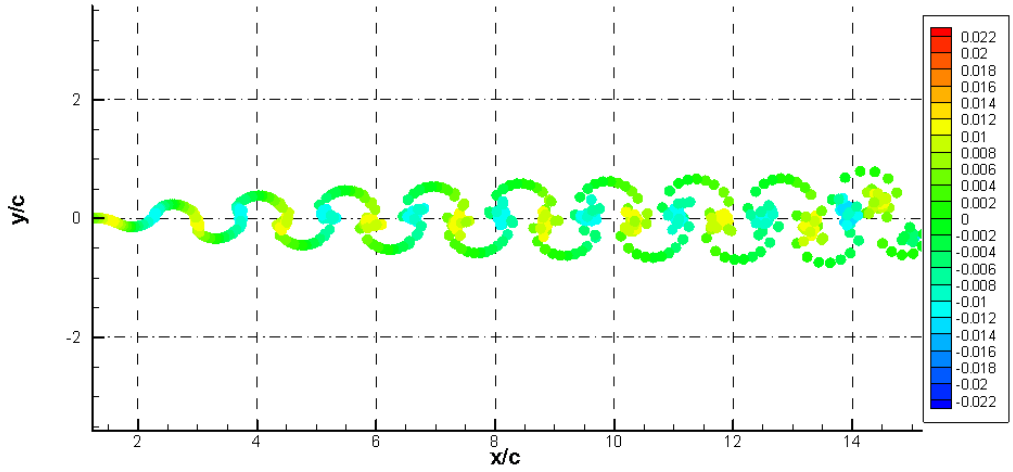

(e) $\overline{E} = 2.4 \times 10^8$

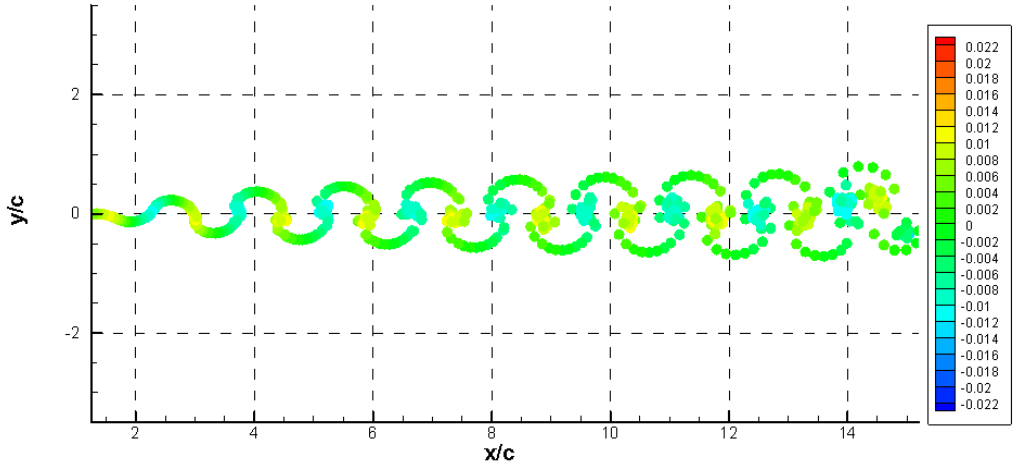

(f) $\overline{E} = 2.8 \times 10^8$

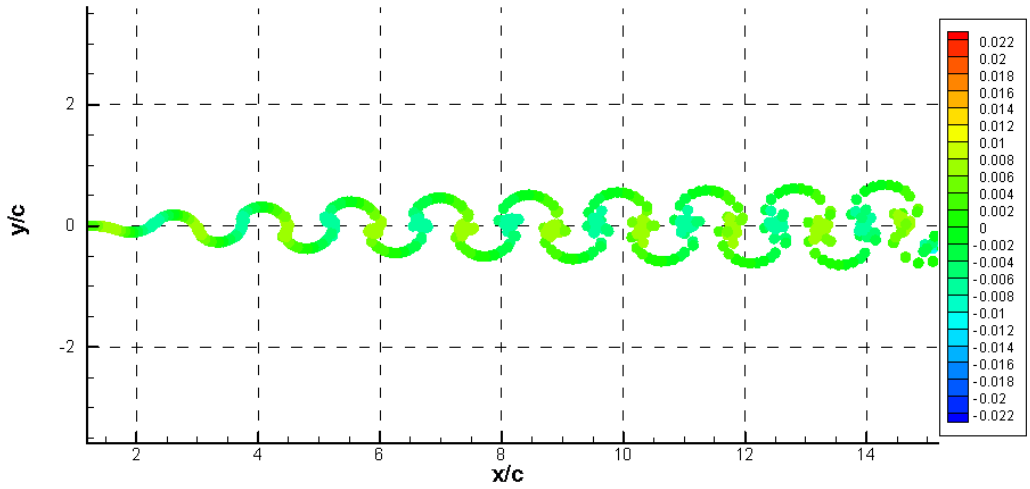

(g) Rigid plate

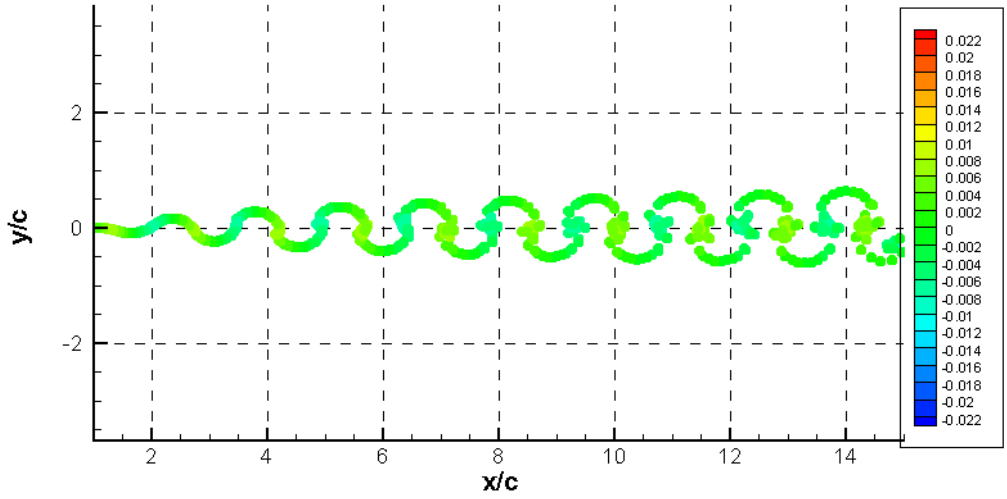

（h）Single rigid NACA0012 airfoil

Figure 9 Wake vortex distribution under different Young's modulus values

VI. Conclusion

In this paper, the fluid-structure coupling problem of a rigid airfoil with an attached elastic plate is numerically simulated by using the unsteady potential flow panel method and the Euler-Bernoulli beam differential equation when the airfoil is in a plunging motion in vertical direction with small amplitude and high frequency. The effect on thrust generation of the fluid-structure coupling is investigated. Some conclusions can be drawn from the analysis of the computed results: (1) For high-frequency and small-amplitude plunging motion, unsteady potential flow panel method has high computational efficiency; (2) Different Young's modulus values of the elastic plate attached to a rigid airfoil will produce significantly different magnitude of aerodynamic forces; The thrust will increase first and then decrease as Young's modulus increases; An optimum unsteady thrust will be produced if a proper Young's modulus value is selected; (3) The efficiency of the thrust also increases first and then decrease as the Young's modulus of the thin plate increases, thus a pertinent Young's modulus value can be found to create best thrust efficiency; (4) Young's modulus of the elastic plate also influences the strength and distribution of the shed vortices in the wake; The maximum thrust of the airfoil corresponds to a largest range of circulation values of the shed point vortices. (5) In the coordinate fixed to the airfoil, the vibration amplitude of the elastic plate attached to the trailing edge increases first and then decrease as Young's modulus increases, and the vibration phase varies with Young's modulus too, that is, as Young's modulus increases, the time point at which the displacement reaches its peak marches backward gradually (that is, moves in the direction of decreasing time).

Acknowledgments

The first author is indebted to Professor Jinsheng Cai for his valuable guidance and is grateful to Mr. Ya Liu, Mr. Lei Zhan, Mr. Jia Xu, and Ms. Chunjun Feng for their helpful suggestions.

References

[1]Spedding, G. R., Lissaman P. B. S., "Technical Aspects of Microscale Flight Systems," *Journal of Avian Biology*, Vol. 29, No. 4, 1998, pp. 458-468.

[2]Knoller, R., "Die Gesetze des Luftwiderstandes," *Flug- und Motortechnik* (*Wein*), Vo. 3, No.21, 1909, pp. 1-7.

[3]Betz, A, "Ein Beitrag zur Erkläerung des Segelfluges," *Zeitschrift fuer Flugtecnik und Motorluftschiffahrt*, Vol. 3, No. 21, 1912, pp. 269-272.

[4]Katzmayr, R, "Effect of Periodic Changes of Angle of Attack on Behaviour of Airfoils," NACA Rept. 147, Oct. 1922.

[5]Koochesfahani, M. M., "Vortical Patterns in the Wake of an Oscillating Airfoil," *AIAA Journal*, Vol. 27, No. 9, 1989, pp. 1200–1205.

[6]Jones, K. D., Dohring, C. M., and Platzer, M. F., "Experimental and Computational Investigation of the Knoller–Betz Effect," *AIAA Journal*, Vol. 36, No. 7, 1998, pp.1240-1246.

[7]Lai, J. C. S., Platzer, M. F., "Jet Characteristics of a Plunging Airfoil," *AIAA Journal*, Vol. 37, No. 12, 1999, pp. 1529-1537.

[8]Shyy, W., Berg, M., and Ljungqvist, D., "Flapping and Flexible Wings for Biological and Micro Air Vehicles," *Progress in Aerospace Sciences*, Vol. 35, No. 5, 1999, pp. 455-505.

[9]Triantafyllou, M. S., Triantafyllou, G. S., Yue. D. K. P., "Hydrodynamics of Fishlike Swimming," *Annual Review of Fluid Mechanics*, Vol. 32, 2000, pp. 33-53.

[10]Heathcote, S., Martin, D., Gursul, I., "Flexible Flapping Airfoil Propulsion at Zero Freestream Velocity," *AIAA Journal*, Vol. 42, No. 11, 2004, pp. 2196-2204.

[11]Heathcote, S., Gursul, I., "Flexible Flapping Airfoil Propulsion at Low Reynolds Number," *43rd AIAA Aerospace Sciences Meeting and Exhibit*, Reno, Nevada, Jan 2005, AIAA Paper 2005-1405.

[12]Tang, J., Viieru, D., Shyy, W., "A Study of Aerodynamics of Low Reynolds Number Flexible Airfoils," *37th AIAA Fluid Dynamics Conference and Exhibit*, Miami, FL, June 2007, AIAA Paper 2007-4212.

[13]Anderson, J. M., "Vorticity Control for Efficient Propulsion," Ph. D Thesis, Massachusetts Institute of Technology and Woods Hole Oceanographic Institution, 1996.

[14]Anderson, J. M., Streitlien, K., Barrentt, D. S., and Triantafyllou, M. S., "Oscillating Foils of High Propulsive Efficiency," *J. Fluid Mech.*, Vol. 360, 1998, pp. 41-72.

[15]Young, J., and Lai, J. C. S., "Oscillation Frequency and Amplitude Effects on the Wake of a Plunging Airfoil," *AIAA Journal*, Vol. 42, No. 10, 2004, pp. 2042-2052.

[16]Liu, J.H., Qiao, Z. D., Yang, X. D., Hao, G. F., "Research of aerodynamic-structure integrative optimization design of wing based on response surface methodology,"[in Chinese] *ACTA Aerodynamica Sinica*, Vol. 24, No. 3, 2006, pp. 300-306.

[17]Teng, N.-H., "The Development of a Computer Code for the Numerical Solution of Unsteady, Inviscid and Incompressible Flow over an Airfoil," M.S. Thesis, Naval Postgraduate School, Monterey, California, 1987.

[18]Liu, D. Z., *Fundamentals of Computational Fluid Dynamics* [in Chinese], Press of Beijing University of Aeronautics and Astronautics, Beijing,1989, pp. 13-14.

[19]Huang, Y. Q., Chen, S. X., *Theory of Mechanical Vibration* [in Chinese], Press of Mechanical Industry, Beijing, 1996, pp. 123.

[20]Anderson, Jr., J. D., *Fundamentals of Aerodynamics*, McGraw Hill Companies, Inc, Boston, 2007, pp.883-925.

[21]Yang. S. C., Luo, S. J., Liu, F., "Computation of the Flows over Flapping Airfoil by the Euler Equations," *43rd AIAA Aerospace Sciences Meeting and Exhibit*, Reno, NV, Jan. 2005, AIAA Paper 2005-1407.

[22]Lai, A., and Liu, F., "Computation of a Rigid Airfoil in Plunging Motion with a Flexible Trailing Beam," *47th AIAA Aerospace Sciences Meeting and Exhibit*, Orland, Florida, Jan. 2009, AIAA Paper 2009-0726.